Dynamic Model Metallo-Supramolecular Dual-Network Hydrogels with Independently Tunable Network Crosslinks

Mostafa Ahmadi [1,2] **Sebastian Seiffert** [2]

[1]Department of Polymer Engineering and Color Technology, Amirkabir University of Technology, Tehran, Iran
[2]Institute of Physical Chemistry, Johannes Gutenberg-Universität Mainz, D-55128, Duesbergweg 10-14, Mainz, Germany
Correspondence to: S. Seiffert (E-mail: sebastian.seiffert@uni-mainz.de)

Received 26 September 2019; Revised 29 October 2019; accepted 12 November 2019
DOI: 10.1002/pola.20190076

ABSTRACT: Hybrid polymer networks emerge between chemical and physical crosslinking, where two different modes of chain connectivity control the material behavior. However, rational relations between their microstructural characteristics, supramolecular kinetics, and the resulting network mechanics and dynamics are not well developed. To address this shortcoming, this study introduces a material platform based on a model dual-network hydrogel, comprising independently tunable chemical and physical crosslinks. The idea is realized by a click reaction between a tetra-PEG and a linear-PEG precursor, whereby the linear block also carries a terpyridine ligand at each end that can form additional physical crosslinks by metal ion–bis(terpyridine) complexation. We change the number of chemical crosslinks by varying the molar mass of the tetra-PEG, and we independently tune the metallo-supramolecular bonds by using different metal ions, Mn^{2+}, Zn^{2+}, Co^{2+}, and Ni^{2+}. Based on that modular approach, we study the rheological behavior and the diffusivity of fluorescent polymeric tracers. The dissociation of the metallo-supramolecular bonds provides a relaxation step, whose timescale and intensity are quantified by a sticky Rouse model. These two characteristics differ not only depending on the metal ion but also according to the chemical network mesh size, which highlights an interplay between the chemical and physical crosslinks. © 2020 The Authors. *Journal of Polymer Science Part A: Polymer Chemistry* published by Wiley Periodicals, Inc. J. Polym. Sci. **2020**, *58*, 330–342

KEYWORDS: click reaction; dual networks; diffusivity; dynamics; rheology; hydrogel; tracer diffusion; supramolecular polymer network

INTRODUCTION Conventional hydrogels are formed from chemically crosslinked polymers. They have the capability to store energy in proportion to their crosslinking density. However, the more they are crosslinked, the sooner they break under mechanical load. A recent approach to combine energy storage and high extensibility is to use double network hydrogels, where a highly crosslinked network is embedded in a loosely crosslinked one.[1] Upon overly strong deformation, the sacrificial breakage of the bonds in the former delays the catastrophic propagation of cracks, while the extensibility of bonds in the latter retains the initial shape.[2] However, since the breakage of chemical bonds is irreversible, once they break, they cannot be further used. To tackle this shortcoming, it has been attempted to replace the brittle network with a physically crosslinked one.[3,4] A wide library of reversible bonds with variable strength and dynamics opens the chance for using these hydrogels as structural and yet adaptive materials.[5] This, however, cannot be realized in a rational fashion unless the relationship between the microstructure and properties of the chemical and physical constitutes and their potential interactions are understood.

The macroscopic properties of conventional chemically crosslinked single polymer networks are controlled by their network structure and its homogeneity. Specifically, it is known that inhomogeneity in the network structure, caused by frozen spatial fluctuations of the crosslinking density, affects the final material properties, particularly in the swollen state.[6–9] To overcome this challenge, Sakai et al. introduced an approach to prepare homogeneous model-network hydrogels through A–B-type click reaction between two monodisperse hetero-functional tetra-PEG precursors.[10] This approach not only provides a new strategy for designing high-strength gels but has also extensively extended the fundamental understanding of classical chemical networks.[11–13]

In contrast to the permanent structure of covalent networks, be it inhomogeneous or model type, the reversibility of

Additional supporting information may be found in the online version of this article.

physical network junctions causes the structure of physical networks to evolve through time[14–16]; it is also an inherent cause for relaxation of these materials upon external load. The dynamics of opening and closing of physical network junctions inherently determines how fast such relaxation or restructuring occurs. A current trend in polymer materials science is to quantify this dependence. In a seminal work, Craig and coworkers demonstrated universality of the time-dependent mechanical response of different supramolecular polymer-network samples by rescaling the timescales of their mechanical spectra with the molecular relaxation times of the utilized physical bonds.[17,18] Later on, Scherman and coworkers provided a more in-depth understanding of the role of the physical bonds on the material properties by decoupling the associative and dissociative processes. They showed that the energetic barrier for dissociation of the supramolecular bonds determines the mechanical strength, while the energetic barrier for association dictates how fast the materials can heal.[19–21] Recently, Olsen and coworkers studied the dynamics of supramolecular bonds in networks using three different techniques: viscoelastic response in rheology, diffusivity of low-molar mass polymeric sticky tracers, and metal exchange experiments on small-molecule supramolecular motifs in dilute solution. With that comparison, they revealed that it is the dissociation process in the gel, and not in the dilute environment, which determines the dynamics of the ligand exchange process and governs the bulk properties of the physical polymer networks.[22]

Despite the aforementioned development of approaches to molecule-to-material design for single polymer networks, the simultaneous effects of the chemical and physical crosslinks on the final properties of double network hydrogels are less explored. Instead, so far, double network hydrogels have been mostly developed based on physical bonds that are inherent in natural polymers or based on synthetic polymers that are randomly functionalized with different supramolecular bonds, including hydrophobic association,[23–25] metal–ligand complexation,[26,27] host–guest interactions,[28] and hydrogen bonding.[29,30] Despite these efforts, still, little is known about the influence of the building blocks, and specifically their dynamics, on the final material properties. This is not only because the utilized structures were not adequately well defined thus far, but also because the independent manipulations in the constructing chemical and physical units were not always possible.

In this regard, Sakai and coworkers have developed a dually crosslinked polymer network based on hydrophilic tetra-PEG blocks and hydrophobic poly(dimethylsiloxane) (PDMS) segments, where the hydrophobic association of PDMS segments serves as the physical crosslinks.[24,25] The association strength could be tuned by changing the ratio of the two building blocks, however, with the cost of affecting the chemical network mesh size. Many other similar dually crosslinked single-network hydrogels based on randomly distributed chemical and physical crosslinks, despite offering remarkable mechanical properties, contain inevitable inhomogeneity of both types of crosslinks.[27] Therefore, a model system comprising homogeneous and independent network components is required to allow for flexible regulation of the kinetics and thermodynamics of the physical bonds without affecting the structure of the chemical network.

To address this challenge, following the introduction of tetra-PEG networks,[10] we develop a model dually crosslinked hydrogel with a homogeneous network structure.[31,32] We use the versatile complexation of different metal ions with terpyridine ligands as the physical linkage. With such a tunable system, we accomplish studying the effects of the chemical and physical contributions to the dynamics of the network independently. We study the network dynamics as reflected in the bulk rheological properties and in the diffusivity of polymeric tracers. The results of that systematic investigation show that there is cooperativity between the chemical crosslinks and the physical bonds. Therefore, building universal master-plots by rescaling the time dimension with the relaxation time of the physical bonds, as it has been demonstrated in physical supramolecular polymer networks,[17,20,22] does not simply work in dual-network hydrogels.

EXPERIMENTAL

Materials

All chemicals are purchased from Sigma-Aldrich(St. Louis, MO, USA) and used without further purification. Tetra-arm hydroxy-terminated PEGs are purchased from Creative PEGWorks. Dry solvents including dimethylformamide, acetonitrile, dichloromethane, and tetrahydrofuran are purchased from Acros.

Synthesis

The model dual-network hydrogels studied in this work consist of a linear PEG precursor that carries both a terpyridine ligand and an *N*-hydroxysuccinimidyl ester at each terminus, and a tetra-arm PEG precursor that contains a primary amine group at each end. The synthesis of each precursor and the terpyridine ligand is explained separately in the following. The synthesis of the polymeric fluorescent tracers for diffusion measurements follows the same approach as it is used for the synthesis of the linear precursor and is detailed further below. All the corresponding ^{1}H NMR and FTIR spectra are gathered in the Supporting Information.

The Linear Precursor

PEG-epoxide. Linear PEG-OH (Sigma-Aldrich; M_w = 6 kg mol^{-1}, PDI = 1.03, 15 g, 5 mmol) is melted at 70 °C and dried *in vacuo* for 1 h, cooled down to room temperature, and then dissolved in dry tetrahydrofuran (250 mL). Sodium hydride (1.65 g, 40 mmol, 60% in mineral oil) is added to the solution and stirred at room temperature for 3 days. Then, epichlorohydrin (7.8 mL, 100 mmol) is added, and the solution is stirred at room temperature overnight. The solution is cooled to 0 °C and quenched with 2 mL of water. Brine is added

(300 mL), and the mixture is extracted with dichloromethane (3 × 400 mL). The organic layer is dried over $MgSO_4$, filtered, and concentrated *in vacuo*. The concentrate is precipitated into cold diethyl ether to obtain the product as a white powder (14.4 g, 96%). ^{1}H NMR (Supporting Information Fig. S1) (400 MHz, DMSO-d_6) δ = 3.70 (s, 1H), 3.33 (s, 38H), 2.72 (t, J = 4.7 Hz, 2H), 1.24 (s, 2H) ppm.

PEG-hydroxy-azide. Sodium azide (3.12 g, 48 mmol) is added to a solution of PEG-epoxide (14.4 g, 4.8 mmol) in dimethylformamide (100 mL), followed by the addition of ammonium chloride (5.1 g, 96 mmol) and stirring at 60 °C for 48 h. The suspension is filtered to remove unreacted sodium azide and ammonium chloride, and the filtrate is concentrated *in vacuo*. The residue is dissolved in dichloromethane (300 mL), then brine (100 mL) is added, and the mixture is extracted with dichloromethane (2 × 300 mL). The organic layer is dried over $MgSO_4$, filtered, concentrated *in vacuo*, and precipitated in cold diethyl ether. The precipitate is collected by filtration and washed with cold diethyl ether to obtain the product as a white solid (12.55 g, 87%). ^{1}H NMR (Supporting Information Fig. S2) (400 MHz, DMSO-d_6) δ = 5.26 (d, J = 5.3 Hz, 2H), 3.67 (s, 1H), 3.40–3.32 (m, 4H), 3.33 (s, 24H), 3.28–3.15 (m, 3H) ppm.

PEG-succinimidyl carbonate-azide. PEG-hydroxy-azide (10 g, 3.3 mmol) is dissolved in 50 mL of dry dioxane. Disuccinimidyl carbonate powder (5.07 g, 20 mmol) is suspended in 20 mL of dry acetone and added to the solution. *4-Dimethylaminopyridine* (2.42 g, 20 mmol) is dissolved in 20 mL of dry acetone and slowly added to the above solution under stirring. The reaction is kept at room temperature for 6 h. The mixture is directly precipitated in cold diethyl ether and dried *in vacuo* overnight. The raw product is dissolved in dichloromethane (50 mL) and washed with 1 N HCl solution (4 × 100 mL) to remove unreacted disuccinimidyl carbonate and *4-dimethylaminopyridine*. The organic phase is precipitated in diethyl ether and dried *in vacuo* to yield the final product as a white solid (8.09 g, 81%). ^{1}H NMR (Supporting Information Fig. S3) (400 MHz, DMSO-d_6) δ = 3.76–3.65 (m, 1H), 3.33 (s, 15H), 2.82 (s, 2H) ppm.

PEG-succinimidyl carbonate-terpyridine. Propargyl-terpyridine (1.15 g, 3.94 mmol) is added to the molten PEG-succinimidyl carbonate-azide (8 g, 2.64 mmol). The molten mixture is stirred overnight at 90 °C under high vacuum. Then, it is cooled to room temperature and dissolved in dichloromethane (20 mL). The solution is precipitated into cold diethyl ether. The precipitated powder is collected by filtration and washed with cold diethyl ether to obtain the product as a white solid (7.5 g, 94%). ^{1}H NMR (Supporting Information Fig. S4) (400 MHz, DMSO-d_6): δ = 8.74 (ddd, J = 4.8, 1.8, 0.9 Hz, 1H), 8.64 (dq, J = 8.0, 1.5 Hz, 1H), 8.11 (d, J = 3.7 Hz, 1H), 8.07–7.98 (m, 1H), 7.52 (dddd, J = 7.6, 4.6, 2.8, 1.2 Hz, 1H), 5.47 (s, 1H), 4.85–4.76 (m, 1H), 3.50 (s, 27H), 3.44 (s, 1H), 3.35 (s, 12H), 2.84–2.74 (m, 3H) ppm. To make sure that the azide group has reacted completely, FTIR spectrometry is conducted before and after grafting of the terpyridine group, in addition to the standard ^{1}H NMR characterization. In this analysis, the absorption at 2100 cm^{-1} addressable to an N_3 group completely disappeared after the reaction (Supporting Information Fig. S5).

To make sure that the presence of the NHS ester group does not affect the grafting efficiency of the terpyridine ligand, due to the spatial hindrance, we change the order of grafting, and first attach the NHS ester and then the terpyridine ligand. The similarity of the obtained ^{1}H NMR spectrum, as shown in the Supporting Information Figure S6 to the one shown in Figure S4 confirms that the reaction efficiency is not affected by the order of grafting.

Propargyl-Terpyridine

Propargyl-terpyridine, which is used in the previous reaction step, is synthesized from the commercially available 2,6-bis (2-pyridyl)-4-pyridone. Dried potassium carbonate (13.3 g, 100 mmol) is suspended in acetonitrile (240 mL). 2,6-Bis (2-pyridyl)-4-pyridone (4 g, 16 mmol) is added to the suspension, followed by the addition of propargyl bromide (3.6 mL, 16 mmol). The brick-red colored suspension is stirred at 60 °C for 24 h. The product is precipitated by pouring the suspension into cold deionized water. The precipitate is collected by filtration, washed thoroughly with cold water, and dried *in vacuo*. The powder is dissolved in boiling *n*-heptane and activated carbon is added (80 mg) under reflux. After a few minutes of mixing, the hot mixture is passed through a hot ceramic filter to obtain the product as yellow fine needle-like crystals (3.23 g, 81%). ^{1}H NMR (Supporting Information Fig. S7) (400 MHz, DMSO-d_6) δ = 8.74 (ddd, J = 4.7, 1.8, 0.9 Hz, 0H), 8.63 (dt, J = 7.9, 1.1 Hz, 0H), 8.24–7.91 (m, 1H), 7.51 (ddd, J = 7.5, 4.7, 1.2 Hz, 0H), 5.11 (d, J = 2.4 Hz, 0H), 3.73 (t, J = 2.3 Hz, 0H), 3.34 (s, 0H), 2.51 (p, J = 1.8 Hz, 1H) ppm.

The Tetra-Arm Precursor

For the preparation of the tetra-PEG precursor, we convert the terminal hydroxyl groups into amines by mesylation and subsequent substitution with ammonia.[33]

Tetra-arm PEG-mesylate. Tetra-arm PEG-OH with a weight-average molar mass of 10 kg mol^{-1} (10 g, 4.0 mmol) is melted at 70 °C under high vacuum to remove traces of water. After cooling to room temperature, the polymer is dissolved in 125 mL of anhydrous dichloromethane, and dry triethylamine (2.5 mL, 18.0 mmol) along with mesyl chloride (1.24 mL, 16.0 mmol) are added to mesylate the hydroxyl end-groups through stirring overnight at room temperature. To remove the unreacted chemicals, dichloromethane (400 mL) and brine (50 mL) are added, and the organic layer is washed with brine (3 × 50 mL), dried over $MgSO_4$, and concentrated *in vacuo*. The residue is precipitated in cold diethyl ether and filtered to yield tetra-arm PEG-mesylate as a white solid (9.8 g, 98%). ^{1}H-NMR (Supporting Information Fig. S8) (400 MHz, DMSO-d_6). δ = 4.33–4.28 (m, 8H), 3.18 (s, 12H) ppm.

Tetra-arm PEG-amine. Tetra-arm PEG-mesylate (9.8 g, 7.8 mmol) obtained in the previous step is dissolved in

ammonium hydroxide (25% aqueous solution, 150 mL) and stirred vigorously for 4 days. The stirring is continued open to the air for another 3 days to evaporate unreacted ammonia. The pH is increased to 13 using a 1 N NaOH solution, and the product is extracted with dichloromethane (DCM) (3 × 100 mL). The obtained solution is dried over $MgSO_4$, filtered, and concentrated *in vacuo*. The concentrate is precipitated in cold diethyl ether to obtain the product as a white solid (7.5 g, 77%). ^{1}H NMR (Supporting Information Fig. S9) (400 MHz, DMSO-d_6) δ = 3.34 (dd, J = 12.3, 6.3 Hz, 2H), 3.32 (s, 6H), 2.64 (s, 1H), 1.75 (s, 1H) ppm.

Synthesis of Fluorescent Tracers

Two different types of fluorescently labeled linear chains are synthesized for diffusivity measurements. Following the reaction steps of the linear precursor, as explained in The linear precursor Section, mono-functional hydroxymethyl ether PEG with a molar mass of 2 kg mol^{-1} is first turned into mPEG-epoxide. Then, the epoxide ring is opened with sodium azide to yield mPEG-hydroxyl-azide, and subsequently, the hydroxyl group is grafted with succinimidyl carbonate. A so-called "non-sticky" tracer polymer (meaning a polymer without terpyridine motifs that could serve for transient attachment to a surrounding hybrid-network matrix also containing that motif) is obtained by reacting the product with (S)-(1)-4-(3-aminopyrrolidino)-7-nitrobenzofurazan dye (NBD). For this purpose, mPEG-succinimidyl carbonate-azide (0.5 g, 0.225 mmol) is dissolved in DMF (5 mL), NBD (0.056 g, 0.225 mmol) is added, and the solution is stirred overnight. The obtained solution is directly precipitated into cold diethyl ether, filtered, and re-precipitated again from DCM into diethyl ether several times to obtain the tracer as a yellow powder. ^{1}H NMR (Supporting Information Fig. S10) (400 MHz, DMSO-d_6) δ = 5.06 (s, 1H), 3.67 (s, 2H), 3.34 (s, 11H), 3.24 (s, 3H), 2.82 (s, 4H) ppm. A so-called "sticky" tracer polymer (meaning a polymer with terpyridine motifs that can serve for transient attachment to a surrounding hybrid-network matrix also containing that motif) is achieved in a similar fashion by replacing the NHS ester with the NBD dye after grafting a terpyridine unit to the mPEG-succinimidyl carbonate-azide. ^{1}H NMR (Supporting Information Fig. S11) (400 MHz, DMSO-d_6) δ = 8.77–8.70 (m, 1H), 8.68–8.60 (m, 1H), 8.10 (d, J = 4.8 Hz, 1H), 8.02 (tdd, J = 7.8, 3.4, 1.8 Hz, 1H), 7.56–7.47 (m, 1H), 5.47 (s, 1H), 4.85–4.76 (m, 1H), 3.52–3.39 (m, 24H), 3.34 (s, 6H), 3.32 (d, J = 5.3 Hz, 1H), 3.24 (s, 2H), 2.84–2.74 (m, 2H) ppm.

Methods

Rheology

Rheological studies are performed on a stress-controlled Anton Paar Physica MCR 301 rheometer with a parallel plate–plate geometry (gap size 1 mm, plate diameter 25 mm). For sample preparation, both precursor polymers are separately dissolved in a buffer solution, added together, and vortexed for a few seconds. Then, the solution is evenly distributed on the lower plate of the rheometer. The upper plate is lowered to have an even distribution of the solution on the upper plate as well. Then, the gap is opened, and the required amount of metal ion solution is added to the polymer solution. Finally, the upper plate is lowered again to reach the desired gap, and the measurement is started.[14,15,32] The standard Anton Paar solvent trap system is used to prevent solvent evaporation, which includes a solvent reservoir and a sealed chamber around the sample. The concentrations of the polymer precursors in buffer and of the metal ions in water are chosen so that the final sample contains a 10% weight fraction of polymer, with an equimolar ratio of the precursors, and a stoichiometric concentration of ions relative to the grafted terpyridine groups. The rheological measurements consist of a time-sweep equilibration period, followed by several frequency sweeps at different temperatures, and finally an amplitude-sweep. Specifically, first a 60-min time-sweep is performed at 25 °C (Υ = 0.05, ω = 10 rad s^{-1}), followed by a 10-min time-sweep at 50 °C (Υ = 0.05, ω = 10 rad s^{-1}), and a 100-min time-sweep at 25 °C (Υ = 0.05, ω = 10 rad s^{-1}). The short, high-temperature time-sweep step in between is included to increase the mobility of the metal ions by decreasing their complexation affinity to the terpyridine groups and therefore to help to provide an even distribution of the metal ions throughout the sample. Subsequently, frequency-sweeps are performed between 10 and 55 °C with 15 °C temperature steps (Υ = 0.05, ω = 500–0.05 rad s^{-1}). In all measurements at a new temperature, the sample is allowed to reach the desired temperature and to equilibrate for 10 min. The reproducibility of the data was proved in a test experiment, up to 40 °C, by repeating the measurement at 10 °C after each measurement at higher temperatures. Finally, an amplitude-sweep is performed at 25 °C at a frequency of 0.1 rad s^{-1} to make sure that the obtained viscoelastic data are in the linear regime.

UV–vis Titration

UV–Vis spectra are recorded on a Cary 300 UV–Vis spectrophotometer (Agilent technologies) at wavelengths between 200 and 800 nm at room temperature. The evolution of the characteristic absorption band of the Ni^{2+}–bis(terpyridine) complex at 324 nm is followed in response to titration with different concentrations of Ni^{2+} ions. Thanks to the very high kinetic stability of the Ni^{2+}–bis(terpyridine) complex,[34] the absorption is expected to reach a steady value when all present terpyridine groups are complexed. From this point, the average number of terpyridine groups grafted to each linear precursor can be calculated. For sample preparation a stock solution of the linear precursor is prepared in water (1 mg mL^{-1}). Solutions of nickel(II) nitrate in water, with different concentrations, are prepared separately so that at the same volume they would provide different molar ratios of the ions to the grafted ligand. The desired volume of the polymer and metal ion solutions are added together and mixed for a 1 h to obtain equilibrated samples.

Fluorescence Recovery after Photobleaching

The diffusive mobility of the sticky and nonsticky tracers within the model dual-network hydrogels is quantified with temporally and spatially resolved fluorescence recovery after photobleaching (FRAP) profiles at 25 °C. The experiments are

conducted on a Leica TCS SP2 confocal laser scanning microscope with a 10× DRY objective of NA = 0.3. The bleached pattern is a line along the *z*-axis of the sample, and hence, a spot in the confocal *x*–*y* plane that fades into the surrounding with a Gaussian radial profile. This profile temporally spreads due to diffusive mixing of bleached and unbleached fluorophores in the bleached region and its surrounding. This diffusion is isotropic and three-dimensional in the sample, but it has effects on the concentration profiles only in the *x*–*y* directions normal to the bleaching line, as no gradient exists or is created in the *z* direction. As a result, a two-dimensional lateral diffusion is recognized. In the scanning mode, the fluorophores are excited with the 488-nm line of an Ar-ion laser at 20% of its maximum power, while full-power irradiation with 6.2 mW is applied in the bleaching period. Before bleaching, a stack of four images is scanned to record the initial condition. Then, a chosen spot is irradiated for 1–3 s with the laser settings mentioned above. As a result, a Gaussian-shaped sink of the fluorescence intensity is created in the spot. After the bleaching, four series of 10 images are recorded to document the fluorescence recovery process with time. Typical temporal steps between single images are 0.5, 1, 2–5, and 5–30 s in the first to the fourth series, respectively. A fifth series of images with a few minutes to 1 h spacing is also recorded for samples that show very slow fluorescence recovery. The FRAP data are analyzed with a multicomponent diffusion model, which provides the bulk-average diffusion coefficient of the tracers.[35,36] For sample preparation, a solution consisting of 98 wt % of tetra-arm precursors and 2 wt % of the selected tracer in DMF is vortex-mixed, and the resulting homogeneous solution is precipitated in diethyl ether, filtered, and dried *in vacuo*. To prepare a network, solutions of the so-obtained tetra-arm precursor and the linear precursor in aqueous phosphate buffer are vortex-mixed at an equimolar ratio, the required amount of metal ions is added, and the sample is spread inside a transparent cell. After solidification, a few drops of silicon oil are added onto the surface of the sample to avoid solvent evaporation. In the final sample, the total concentration of the tracer is less than 1 wt %, which corresponds to 1.2 mol % of the tracer relative to the total terpyridine ligands. Due to that low fraction of tracers, the presence of double tracers formed by association of two linear tracers, and the imperfection they bring to the dually crosslinked network, can be ignored.

RESULTS AND DISCUSSION

Preparation of the Model Dual-Network Hydrogels

The purpose of this study is to synthesize and evaluate the dynamics of a model dual-network hydrogel, where chemical and physical crosslinks can be independently tuned. In a former publication, we had already modified the tetra-PEG approach, as developed originally by Sakai and coworkers, by grafting physical crosslinks to one of the precursors.[32] Here, we update our former approach by simplifying the synthesis steps and improving the overall efficiency. Specifically, we functionalize a linear PEG precursor to carry an *N*-hydroxysuccinimidyl (NHS) ester and a terpyridine ligand at each end and modify a tetra-arm PEG precursor to have terminal amine groups, as shown in Scheme 1. The reaction between the NHS ester and primary amines is a well-known quantitative click bioconjugation,[37] which provides the chemical linkages of the model network as soon as they are mixed in water. At the same time, the terpyridine groups form the metallo-supramolecular bonds through metal ion–bis(terpyridine) complexation, upon introduction of metal salts in water.

The branching point of each star precursor serves as one chemical crosslink of the network, as illustrated in Scheme 1. Accordingly, a network strand is composed of two arms of the two different star precursors plus a linear precursor in between that links them. Therefore, a larger number of chemical crosslinks per volume corresponds to a network made of more but smaller star precursors, which results in a smaller network mesh size.

Our former experience with grafting an NBD dye and a terpyridine moiety at the same end of a tetra-PEG through activation by *p*-nitrophenyl chloroformate shows that the bulky terpyridine group does not shield the hydroxyl group in the subsequent grafting with bulky chloroformate ester.[35] To make sure that the presence of the first bulky group, that is, the NHS ester, does not affect the grafting efficiency of the second group, that is, the terpyridine ligand, either, here we change the order of grafting the NHS ester and the terpyridine groups on a linear PEG precursor with 6 kg mol^{-1} molar mass. Since the ^{1}H NMR spectra of the final products are quite similar (compare Figs. S4 and S6 in the Supporting Information), we compare the time evolution of the dynamic moduli of their corresponding chemical networks formed in combination with a 10 kg mol^{-1} tetra-PEG precursor, coded as LP6SP10-NHS-TPy and LP6SP10-TPy-NHS. The storage modulus is an indicator of the number of chemical crosslinks, which provides an insight into the number of grafted NHS ester units. For this purpose, we follow a time-sweep oscillatory measurement (Υ = 0.05, ω = 10 rad s^{-1}) until the storage modulus reaches a steady equilibrium level, as shown in Figure 1(a). The obtained storage modulus is only 5% larger when terpyridine is grafted first. This finding shows that the number of chemical crosslinks, and therefore, the number of NHS ester groups, is not significantly affected by the order of grafting.

In addition, to quantify the number of grafted terpyridine groups, we determine the steady equilibrium modulus in presence of different molar ratios of Ni^{2+} ions, in a similar fashion (time-sweeps with Υ = 0.05, ω = 10 rad s^{-1}). The equilibrium modulus rises with a steep slope upon addition of Ni^{2+} ions, because they form strong transient bonds with the grafted terpyridine units, as shown in Figure 1(b). This raise stops and the curve flattens as the number of present Ni^{2+} ions precedes the stoichiometric ratio compared to the expected number of terpyridine groups. This may look surprising because it was reported that in the molten state, the plateau modulus increases steadily by introducing further Ni^{2+} ions beyond the stoichiometric ratio. This was associated with the complexation of the excess metal ions with the oxygen atoms of the

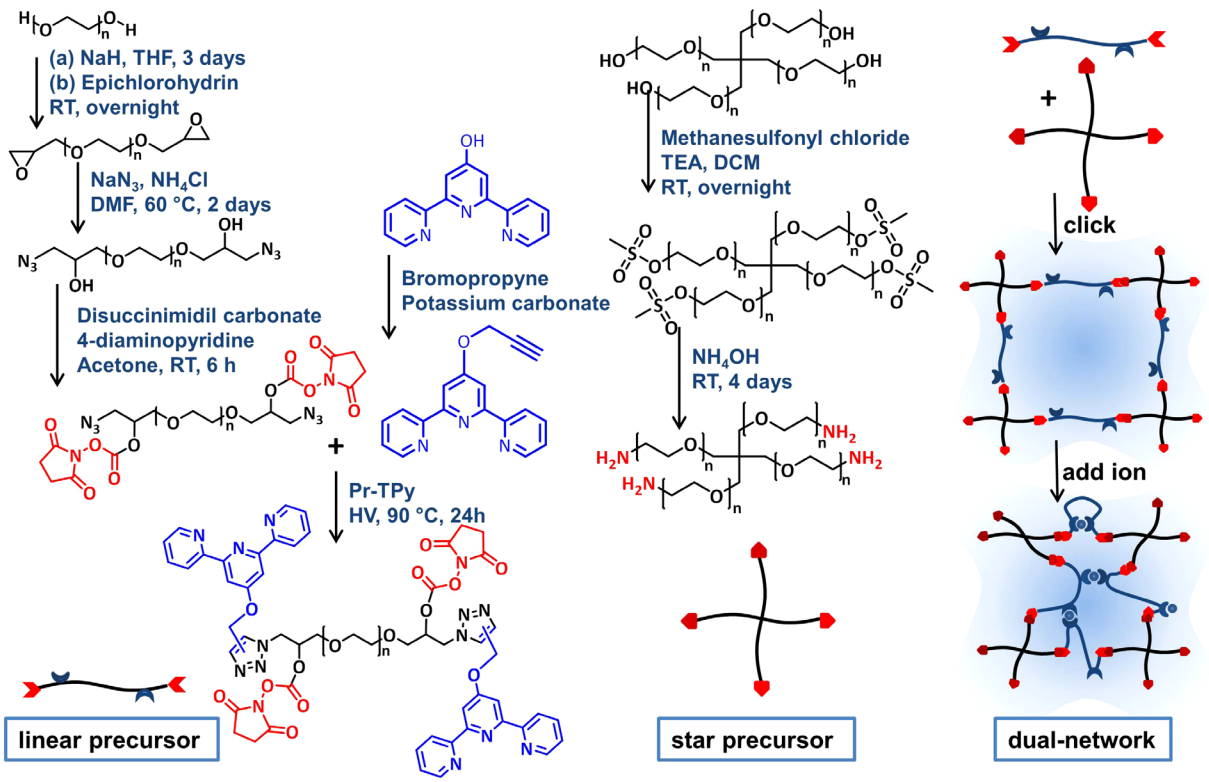

SCHEME 1 Synthesis approach for preparation of a model dual-network hydrogel out of a linear and a tetra-arm star-shaped precursor. The linear precursor is a hydroxyl-terminated PEG first functionalized with epoxide rings that are subsequently opened to yield hydroxyl and azide groups at both chain ends, which are in turn, grafted with NHS ester and terpyridine ligands. The star precursor is a hydroxyl-terminated tetra-arm PEG functionalized by amine groups through mesylation and subsequent substitution with ammonia. A chemical network instantaneously forms by click reaction between the NHS ester and amine groups when these precursors are mixed in water. The metal ion-bis(terpyridine) metallo-supramolecular bonds form upon addition of a metal salt. [Color figure can be viewed at wileyonlinelibrary.com]

PEG backbone.[38] However, our results show that in a dilute state, the formation of such extra linkages is not significant. To confirm the above argument, we titrate the terpyridine groups with nickel nitrate salt in water. Specifically, the characteristic absorption of the Ni^{2+}–bis(terpyridine) complex band increases by adding Ni^{2+} ions until a plateau is reached when no terpyridine group is available any more for further complexation.[39] Accordingly, this plateau is reached at the stoichiometric ratio of Ni^{2+} compared to the expected number of terpyridine ligands, as also shown in Figure 1(b). Conclusively, the number of the grafted terpyridine groups is close to what was planned in the synthesis.

To provide physical crosslinks with tunable strength and dynamics, we use nitrate salts of manganese(II), zinc(II), cobalt(II), and nickel(II). By introduction of these salts into the precursor solutions, each metal ion complexes to two terpyridine ligands with equilibrium constants that vary in the order of Mn < Zn < Co < Ni.[14,15,40,41] Hoyler et al. have shown that the equilibrium constant of complexation with unsubstituted terpyridine increases about two orders of magnitude by going from one ion to the next stronger one in that series.[41] The very low dissociation constant of the strong Co^{2+} and Ni^{2+} ions infers that establishing equilibrium conditions by a homogeneous distribution of the ions throughout the sample takes a very long time. Both the association and dissociation reaction rates increase with temperature, as they follow Arrhenius-type temperature dependencies. However, since the dissociation process has a higher activation energy than the association process,[41] its relative increase is significantly stronger. Therefore, the mobility of small-molecule ions can be effectively amplified by increasing the temperature.[15,41] Consequently, we follow a specific equilibration period in our rheology experiments before starting the actual measurements, which includes a short-term high-temperature time-sweep between two long-term room-temperature ones.

We use small-amplitude oscillatory shear (SAOS) rheological measurements to study the dynamics of the model dual-networks. For this purpose, premixed precursor solutions are placed between the rheometer plates, and after once closing and re-opening the gap, an ion solution is distributed on the surface in a dropwise fashion. SAOS measurements are carried out after the equilibrium condition is reached, as demonstrated by reaching a steady storage modulus using the

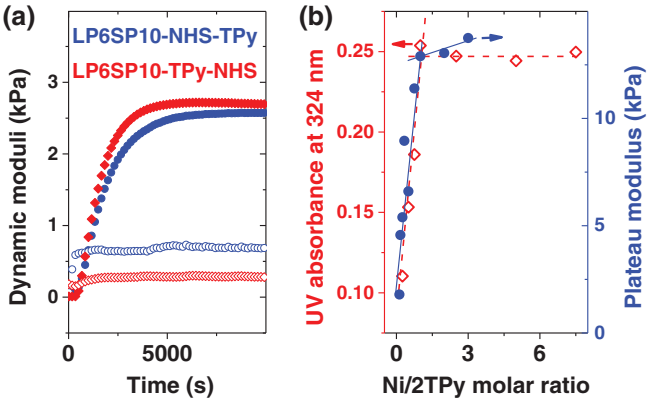

FIGURE 1 (a) Time-evolution of the dynamic moduli of samples with different orders of NHS ester and terpyridine grafting during the precursor polymer synthesis. (b) Equilibrium modulus, as obtained in a time-sweep oscillatory measurement (right ordinate, $\Upsilon = 0.05$, $\omega = 10$ rad s^{-1}), and the characteristic Ni^{2+}–bis(terpyridine) complex UV–Vis absorption at 324 nm (left ordinate), as a function of the stoichiometric ratio of Ni^{2+} ions compared to terpyridine, for a dual-network comprising LP6 and SP10 precursors. [Color figure can be viewed at wileyonlinelibrary.com]

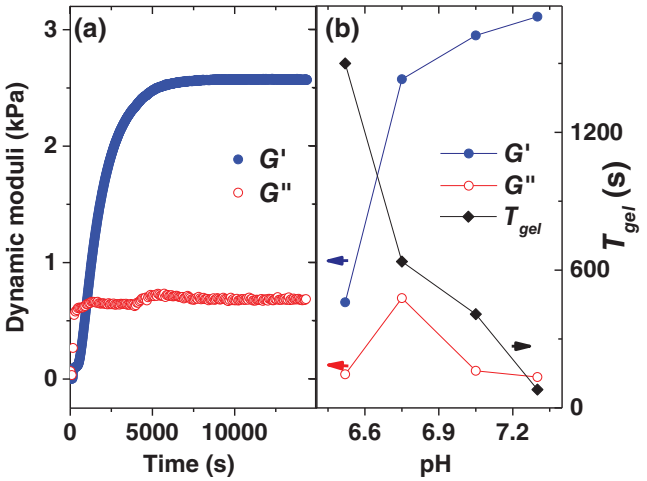

FIGURE 2 (a) Formation of a chemical network between LP6 and SP10 precursors at a pH value of 6.75, as assessed by rheological time-sweep experiments at $\Upsilon = 0.05$, $\omega = 10$ rad s^{-1}; the gelation time is determined based on the G'–G'' crossover time. (b) Dependence of the steady storage and loss moduli and the gelation time on the buffer pH value. [Color figure can be viewed at wileyonlinelibrary.com]

aforementioned time-sweep protocols. This process requires an optimal gelation time so that on one hand, molecular-level mixing is achieved, and more importantly bubbles formed during vortex-mixing of the solutions escape before the concentration gradients are frozen by gelation, while on the other hand, the equilibrium network structure is realized in a reasonable time before the NHS ester groups become unavailable due to hydrolysis. The click reaction between the NHS ester and the amine group is almost instantaneous, and gelation is achieved in water in less than a minute. In this regard, Sakai et al. have shown that this click reaction does not proceed at highly acidic or highly basic conditions, due to excessive protonation of the amine groups or hydrolysis of NHS ester, respectively.[42] Therefore, we first find the optimal gelation time by adjusting the pH value. For that purpose, phosphate buffers with different pH values are prepared by mixing various ratios of 50 mM aqueous solutions of NaOH and monopotassium phosphate. The gelation time is comprehended from the G'–G'' crossover in a time-sweep measurement at room temperature, as shown in Figure 2(a). The evolution of the steady storage and loss moduli and the gelation time as a function of pH are shown in Figure 2(b). The storage modulus increases with pH, however, with considerably shallower slope at high pH values, while the gelation time decreases monotonically. Accordingly, the network-forming reaction works more efficiently at physiological pH values; however, to assure that the required mixing time is employed, a pH value of 6.75 is subsequently used for the preparation of all samples.

Dynamics of Dual-Network Hydrogels

To demonstrate the independent tunability of the chemical and physical linkages in the proposed model dual-network hydrogels, we use a linear precursor with a molar mass of 6 kg mol^{-1} (coded as LP6) and three tetra-arm precursors with molar masses of 5, 10, and 20 kg mol^{-1} (respectively, coded as SP5, SP10, and SP20), in combination with stoichiometric amounts of the aforementioned metal ions. An overall concentration of 100 g L^{-1} is selected to assure that both precursors are present above the overall overlap concentration.[10,15] The corresponding dual-networks are coded as LP6SPXM, where X denotes the molar mass of the tetra-arm precursor and M indicates the utilized metal ion. Oscillatory shear experiments are performed at four temperatures from 10 to 55 °C with 15 °C steps, and the representative measurements at 25 °C are shown in Figure 3.

The dynamic moduli of the reference chemical network demonstrate a flat storage modulus that overlays for all temperatures. This signifies the absence of any relaxation mechanisms in the studied frequency domain. In contrast, the dual-network hydrogels exhibit a relaxation process in the presence of the metal ions, which can be comprehended from a peak in the loss modulus. This relaxation is attributed to the ligand exchange process of the metal ion–bis(terpyridine) complexes. The relaxation peak is located above the experimentally accessible frequency range for the LP6SP10Mn sample, consistent with the observation that adding Mn^{2+} ions to the precursor solution does not significantly increase the viscosity of the sample. However, the relaxation process can be distinguished for the LP6SP10Zn and LP6SP10Co samples. The Maxwell-type relaxation peak is fully visible for the former, while it is partially below the accessible frequency range for the latter. The LP6SP10Ni sample behaves like a pure chemical network with flat storage moduli. Consequently, the dissociation time of the corresponding metal ion–bis

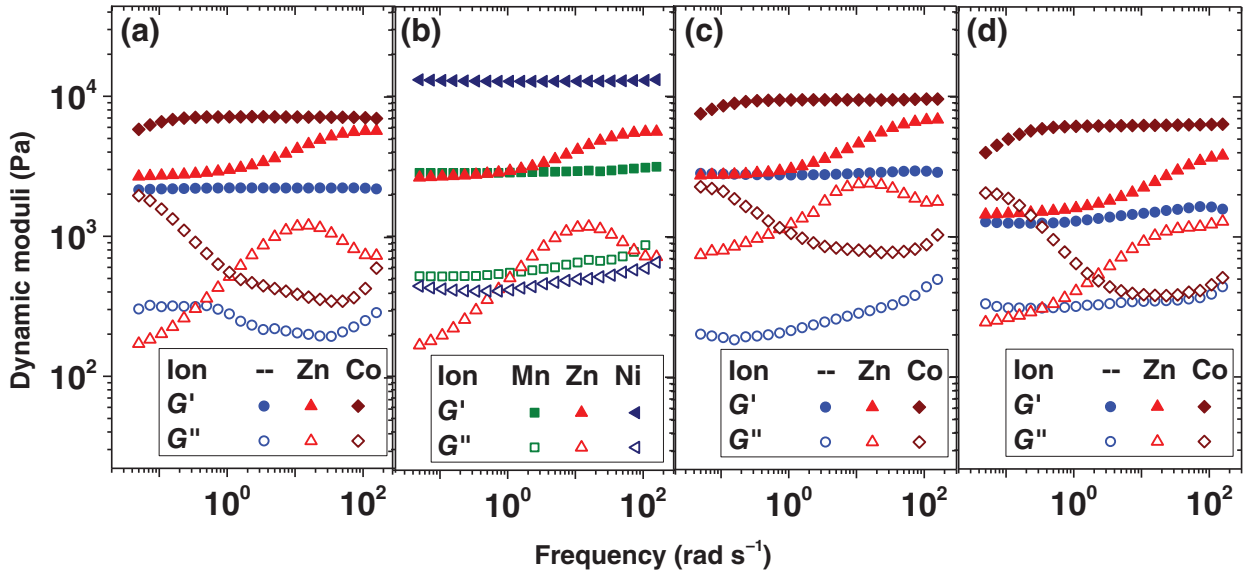

FIGURE 3 Dynamic moduli of the dually crosslinked networks in presence of different metal ions for (a,b) LP6SP10M (c) LP6SP5M, and (d) LP6SP20M, at a representative temperature of 25 °C. [Color figure can be viewed at wileyonlinelibrary.com]

(terpyridine) complexes is located below the accessible frequency range, except for the high-temperature measurements, which show a decline in the storage modulus at low frequencies. In addition, the storage moduli of the dually crosslinked networks are larger than that of the plain chemical network at frequencies above the inverse dissociation time of the supramolecular complexes. The difference between the storage moduli of the chemical network and the dually crosslinked ones increase when stronger ions are used for the terpyridine-complexation in the order of Zn < Co < Ni. Similar relaxation processes can be observed in the dynamic moduli of the dual-network hydrogels made from the SP5 and SP20 tetra-arm precursors in the presence of Zn^{2+} and Co^{2+} ions, as shown in Figure 3. However, the relaxation times of the same metal–ligand complexes do not match in networks made from differently sized star-shaped precursors.

To provide a more quantitative understanding about the interplay between the chemical and physical network linkages, we model the observed relaxation process by a simple sticky Rouse mechanism.[43–45] The Rouse model is originally developed to explain the relaxation of unentangled polymer chains in dilute solutions. Later on, it was incorporated in tube models for polymer melts, to explain the relaxation of polymer segments that are smaller than the tube diameter.[46] Longer ranges of Rouse relaxation are not possible since that involves dragging the neighboring entangled chains. In a swollen network like our system, with an ideally homogeneous structure, the relaxation of strands between chemical linkages follows a three-dimensional Rouse process. The scale of Rouse-like relaxation starts from a monomer and proceeds to the whole strand length in the case of a chemical network. Further relaxation is prohibited by the chemical linkages. In the case of a dual-network, however, Rouse modes proceed until the average length between linkages that are formed by either chemical or physical crosslinks. Further relaxation beyond this scale is delayed by the dissociation time of the metallo-supramolecular bonds.

In the simple sticky Rouse model, the network is replaced by an arbitrary long linear chain with an entanglement length equal to the strand length between two chemical linkages. Three different types of Rouse relaxation modes are assumed; (a) modes for length scales smaller than a strand length, formed by the chemical or physical linkages, proceed by monomeric friction; (b) modes beyond this and below the strand length between two adjacent chemical linkages proceed by supramolecular friction; and (c) modes beyond that are frozen due to the infinite relaxation time of the chemical crosslinks:

$$\varphi_{\text{fast}}(t) = \sum_{p=z_t+1}^{N} \exp\left(\frac{-2p^2 t}{\tau_{R,\text{fast}}}\right) \quad (1)$$

$$\varphi_{\text{sticky}}(t) = \sum_{p=z}^{z_t} \exp\left(\frac{-p^2 t}{\tau_{R,\text{sticky}}}\right) \quad (2)$$

$$\varphi_{\text{infinite}}(t) = \sum_{p=1}^{z} \exp\left(\frac{-p^2 t}{\tau_{R,inf}}\right) \quad (3)$$

The utilized timescales are therefore defined as:

$$\tau_{R,\text{fast}} = \tau_e z^2 \quad (4)$$

$$\tau_{R,\text{sticky}} = \tau_{es} z^2 \quad (5)$$

$$\tau_{es} = \max\left(\tau_e, \tau_{\text{ex}}\left(\frac{M_e}{M_{\text{bin}}}\right)^2\right) \quad (6)$$

$$\tau_{R,inf} = \infty \quad (7)$$

where τ_{ex} and τ_e are the effective dissociation time of the supramolecular complexes and the Rouse relaxation time of

an entanglement, respectively. Accordingly, M_{bin} and M_e are the molar mass of the strands between two adjacent supramolecular associative groups and two neighboring chemical linkages. Finally, z, z_t, and N denote the number of entanglements, that is, the chemical crosslinks, the total number of linkages formed by the chemical and physical crosslinks, and the degree of polymerization. The transient modulus is calculated as:

$$\frac{G(t)}{\nu RT} = \frac{1}{z}\left(\varphi_{fast}(t) + \varphi_{sticky}(t) + \varphi_{infinite}(t)\right) \quad (8)$$

where ν is the density of entanglement, that is, the chemical crosslinks, which can be calculated based on the molar concentration of the tetra-arm precursor. The νRT term in the denominator of the left side is expected to reflect the plateau storage modulus of the chemical network before addition of the metal ions. Following our earlier works,[47,48] we use Schwarzl's approximation to convert the transient modulus into dynamic moduli. The model is applied to rheological measurements at different temperatures, and the fit parameters, including the number of active supramolecular associative groups per strand and their corresponding lifetimes, are found by the Nelder–Mead optimization method.[49]

Before applying the model, the theoretical storage moduli of the chemical networks based on the affine network assumption are evaluated. In this approach, the number of chemical crosslinks is determined based on the molar concentration of the tetra-arm precursors. Interestingly, the experimental values are more than twice of the theoretical expectations, as shown in the main plot of Figure 4. Accordingly, the star precursors are not the only source of effective network linkages, and probably, trapped entanglements or hydrophobic association of terpyridine ligands provides similar contributions to the storage modulus. This is not surprising since even in the case of the LP6SP5 sample with the smallest mesh size, the strand length is longer than the entanglement molar mass of PEG,[38,50] and the system is above the overlap concentration. Consequently, the νRT term in eq. 8 is replaced by the experimentally measured storage modulus of the corresponding chemical networks.

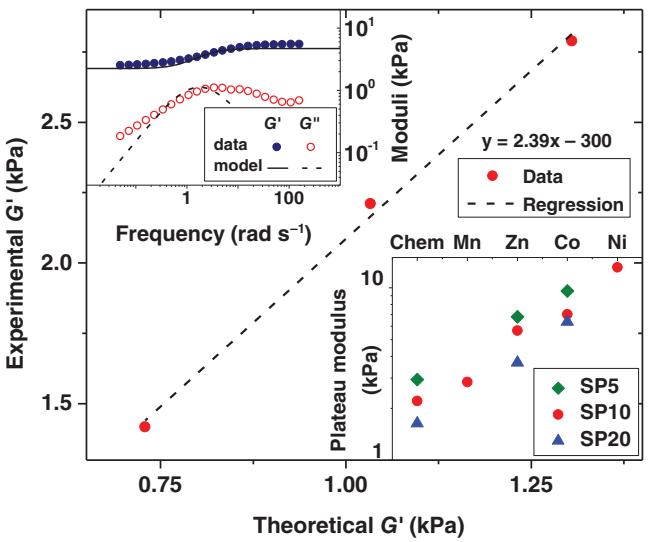

FIGURE 4 Experimentally measured storage moduli of networks formed by the SP5, SP10, and SP20 tetra-arm precursors against the theoretical expectations based on the affine network assumption ($G = \nu RT$) (main plot), along with the detailed predictions provided by the sticky Rouse model for the LP6SP10Zn sample at 10 °C (top-left inset plot) and the storage moduli of different network structures in the presence of different ions ($T = 25$ °C, $\Upsilon = 0.05$, $\omega = 108$ rad s^{-1}, down-right inset plot). [Color figure can be viewed at wileyonlinelibrary.com]

The number of metallo-supramolecular bonds is limited to a maximum of two bonds per network strand, as illustrated in Scheme 1. Therefore, the maximum storage modulus is achieved when all the ligands are actively participating in network formation. This happens when the utilized metal ions form metallo-supramolecular bonds with long lifetimes. A larger plateau modulus cannot be achieved based on this simple binary-association picture. Surprisingly, the plateau moduli increase monotonically in all our network structures, as shown in the lower inset plot of Figure 4. Hence, we use the proposed sticky Rouse model to gain a quantitative insight into the nature of physical bonds.

The proposed simple model provides a decent match to the experimental data in the vicinity of the relaxation of the metallo-supramolecular bonds, as shown in the upper inset plot of Figure 4. However, it shows a significant mismatch to the loss modulus in the frequency region between the fast and the slow sticky modes, as already reported for similar systems.[44,45,51] The reason is that the model contains no source of relaxation in this region, while in reality, dangling ends, loops, and other connectivity defects can relax in between.[44,52] Fortunately, this does not interfere with our target of studying the temperature dependence of the number and lifetime of the metallo-supramolecular bonds. The obtained τ_s values follow an Arrhenius-type dependence on temperature, and therefore activation energies can be obtained by linear regression, as shown in Figure 5. There are limitations in deriving the lifetimes of metallo-supramolecular bonds that dissociate beyond the accessible frequency ranges; therefore, the LP6SP10Mn sample cannot be studied this way, and the LP6SP10Ni sample can be analyzed only at higher temperatures. The obtained association time at 40 °C for this sample is the minimum value that is required to capture the observed behavior, and the actual value should be even higher, which corresponds to larger activation energy.

The trends in the obtained activation energies for networks based on Zn^{2+} and Co^{2+} ions suggest that there is a cooperativity between the chemical and metallo-supramolecular bonds in the whole relaxation process. This cooperativity can be unveiled by studying the dissociation activation energies as a function of the network mesh size, as illustrated in Figure 6 (a). The activation energy seems to decrease monotonically with the mesh size for networks based on Zn^{2+} ions. This suggests that there is a larger energetic barrier against relaxation

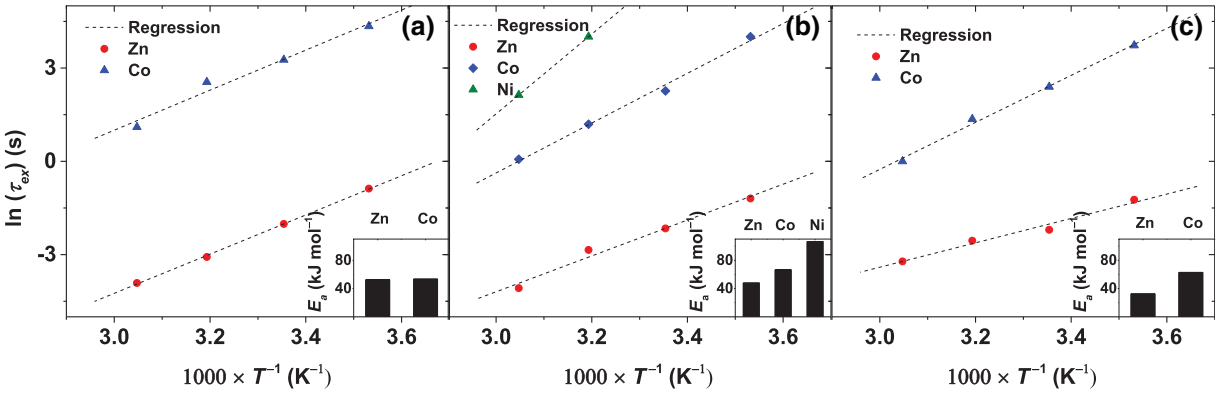

FIGURE 5 Linear regression of the metallo-supramolecular bond lifetimes derived from the sticky Rouse model against the inverse temperature for (a) LP6SP5M, (b) LP6SP10M, and (c) LP6SP20M model dual-network hydrogels (main plot) and the obtained dissociation activation energies (inset plots). [Color figure can be viewed at wileyonlinelibrary.com]

in case of a network with smaller mesh size. Simply put, the bis-complexes based on Zn^{2+} are more kinetically stable when the terpyridine groups are closer together. We hypothesize that this is because the thermal fluctuations of the polymer network strands pull the complexes on their telechelic joints apart and thereby facilitate their breaking, which is more pronounced for longer strands than for shorter ones, as the longer strands have larger fluctuations scales than the shorter. This hypothesis is based on a related finding made in a telechelic metallo-supramolecular linear polymer system, for which we have demonstrated that the lifetime of the metal–ligand complex decreases with increasing length of the polymer precursor attached to it.[50] Moreover, in a network with a smaller mesh size, the possibility of coming back to the same partner after breakage is larger. For the Co^{2+} ion, on the contrary, the activation energy seems to stay steady. This is interpretable by considering the bis-complexes based on Co^{2+} strong enough so that the network strand length cannot affect their kinetic solidity.

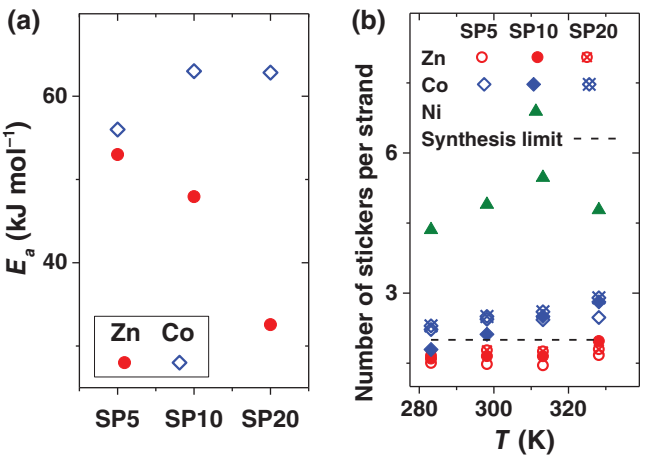

FIGURE 6 (a) Dissociation activation energies of the dual-network samples formed by Zn^{2+} and Co^{2+} ions. (b) Effective number of metallo-supramolecular bonds per network strand of the dual-network samples as a function of temperature. [Color figure can be viewed at wileyonlinelibrary.com]

The other important parameter of the sticky Rouse model is the average number of noncovalent associations. The PEG strands between chemical linkages contain two terpyridine groups. However, not all of them effectively participate in the formation of bis-complexes. In fact, according to the thermodynamic equilibrium constants of the utilized ion, a fraction of metal ions and terpyridine ligands are in the mono-complex or even in the fully dissociate state.[53] Consequently, the number of effective metallo-supramolecular groups should be equal to or less than two. Accordingly, the number of supramolecular linkages that is required for capturing the high plateau level is between 1.5 and 2 for the networks made by Zn^{2+}, as shown in Figure 6(b). In contrast, the number of required metallo-supramolecular linkages proceeds beyond 2 for the networks made by Co^{2+} and even reaches 5 for the ones made by Ni^{2+}. These results indicate that, depending on the utilized ion, supramolecular assemblies larger than what is expected from a simple binary association can form. Such behavior has been frequently reported for supramolecular polymer systems in melt and it has been associated with different polarity of polymer backbone and supramolecular motifs.[38,44,54–57] In our hydrogel system, however, it can be speculated that the formation of nanoscopic clusters can be mediated by Coulomb interactions between the charged bis-complexes in the gel and the counter ions in their vicinity.[58] This of course depends on the association tendency of the metal ion and the dielectric constant of the solvent. The number of associations slightly increases with temperature, which could be due to the straight temperature dependence of the storage modulus itself, as comprehended from the $G = \nu RT$ equation.

To provide a molecular-level insight into the studied relaxation process, we investigate the diffusivity of a low-molar mass polymeric tracer with or without a terpyridine anchor within the model dual-network samples formed by the SP10 precursor. This is accomplished by fluorescence recovery after photobleaching performed on a confocal laser scanning

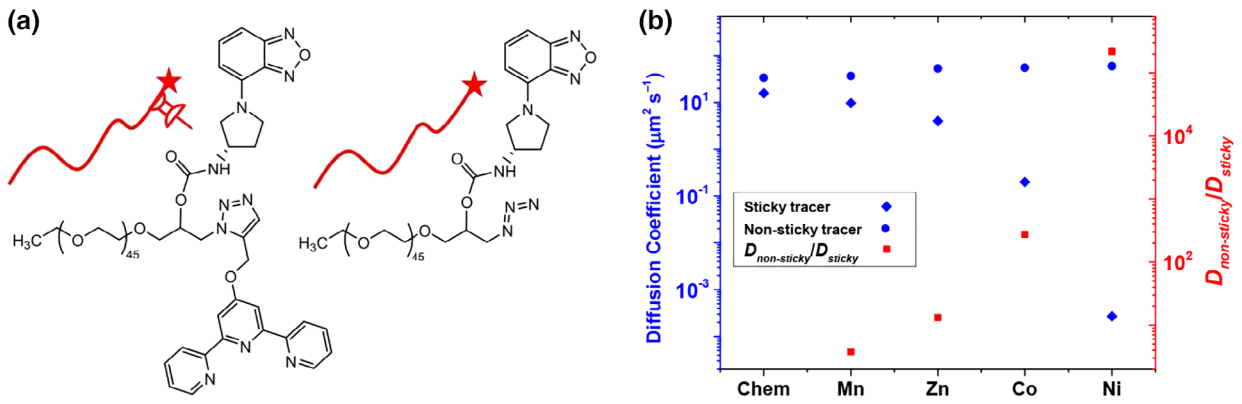

FIGURE 7 (a) Chemical structure of the synthesized fluorescent dye-labeled sticky and nonsticky polymeric tracers. (b) Diffusion coefficients of the sticky and nonsticky tracers within the model networks. The right ordinate shows the ratio of the two diffusion coefficients, which scales with the association lifetime of the metallo-supramolecular complexes. [Color figure can be viewed at wileyonlinelibrary.com]

microscope. For this purpose, a fluorescent dye-labeled linear tracer is synthesized in a similar approach as followed to make the linear precursor, with minor adjustment. In detail, a mono-functional PEG with a molar mass of 2 kg mol^{-1} is functionalized with both NHS ester and azide groups at the functional end. A nonsticky tracer is simply obtained by carrying out the click reaction between the NHS ester and the amine-functional NBD dye, similar to the reaction that was used to form the chemical crosslinks of the hydrogels. This nonsticky tracer is small enough to simply diffuse through the network. As a complement, a sticky tracer is obtained through the same grafting process after connecting a terpyridine ligand to the neighboring azide functional group. This sticky tracer binds to the network by metal complexation and only diffuses through the network in a temporarily liberate state. The structures of both tracers are illustrated in Figure 7(a), and the corresponding ^{1}H NMR spectra are provided in the Supporting Information Figures S10 and S11.

The diffusion of these tracers is studied by first bleaching the fluorophores in a selected μm-sized spot in the sample, using a high-intensity laser beam, and then observing the temporal and local evolution of that darkened spot. The dark pattern smears into the surrounding by diffusive motion of the bleached and unbleached tracers from and into the dark region, respectively. The intensity profiles are fitted by Gaussian distribution functions, which allow determining the distribution of the diffusion coefficients that causes the bleached spot smearing.[36,59]

The unentangled nonsticky tracer is expected to simply diffuse through the network meshes by Brownian motion. The diffusion coefficient is not affected by the presence of metal ions because there is no interaction between the nonsticky tracer and the metallo-supramolecular complexes in the surrounding network. Accordingly, the diffusion coefficients obtained for the chemical and the dual-network hydrogels are very close to each other, as shown in Figure 7(b). The sticky tracer, in contrast, is slowed down by repetitive complexation of the grafted ligand to the surrounding network. Consequently, the obtained diffusion coefficients decrease significantly by utilizing strongly associating metal ions, in the order of Mn < Zn < Co < Ni, as also shown in Figure 7(b).

Both tracers follow a similar translational diffusion through the network according to Brownian motion. The sticky tracer, however, spends a significantly longer time in the associated state. Therefore, its overall diffusion coefficient correlates with a combination of the translational motion and the association time. Accordingly, the ratio of diffusion coefficients ($D_{\text{nonsticky}}/D_{\text{sticky}}$) scales with the association time of the metallo-supramolecular bonds, τ_s. The obtained data are shown by the right ordinate of Figure 7(b). The obtained results follow the same order that was revealed from the rheological data. This is a molecular scale confirmation of the results that are obtained from the macroscopic rheological properties. However, the metallo-supramolecular bond formed between the sticky tracer and the network through Ni^{2+} appears to be more kinetically stable at room temperature than expected from rheology. Evidently, the rheological analysis is not capable of unveiling the relaxation process of the dual-network systems made by Ni^{2+}, as the corresponding association time is more than two orders of magnitude larger than the one formed in presence of the weaker Co^{2+} ion. These relaxation times are in good agreement with the inverse of dissociation rate constants, which was determined for the complexation of small-molecule terpyridine ligands with different metal ions using UV spectrometry, specifically for Ni^{2+} and Co^{2+}.[14,15,41]

CONCLUSIONS

Fundamental understanding of the molecular design of single polymer networks is profound not only for traditional chemical networks but also for transient networks formed by supramolecular bonds. Our systematic investigation on the new class of dynamic dually crosslinked networks reveals that the typical structure–property relationships are not directly applicable to these hybrid systems, though. Our study is realized

by devising a model dual-network system, where the extent of chemical crosslinks and the dynamics of metallo-supramolecular bonds can be independently varied. For this purpose, chemical networks with different mesh sizes are synthesized and additional metallo-supramolecular bonds with variable strength are incorporated using different metal ion–bis(terpyridine) complexes. Rheological analysis confirms that the number and association time of the metallo-supramolecular bonds follow their thermodynamic equilibrium constants that were already derived based on complexation with unsubstituted terpyridine ligands, that is, $Mn^{2+} < Zn^{2+} < Co^{2+} < Ni^{2+}$. However, depending on the supramolecular bond strength, the number and lifetime of the bis-complexes change by the network mesh size. Specifically, the dissociation activation energy decreases with the network mesh size for dual-networks made by Zn^{2+} ions. This is attributed to the larger fluctuation of the longer polymer network strands compared to the shorter ones, which more effectively pulls the metallo-supramolecular bonds along them out of complexation. Moreover, stronger ions form a larger number of associations compared to what is expected from the synthesis, which is attributed to the formation of collective assemblies through nanoscopic clustering. A molecular-level confirmation of the observed behavior is provided by studying the diffusivity of low-molar mass polymeric tracers. The diffusion of a nonsticky tracer is not affected by the network structure, while a sticky tracer is slowed down by the same order that is expected from the rheological analysis. These results underline the importance of the interplay between chemical and physical bonds in hybrid gels, which should be considered for the development of materials based on this concept.

ACKNOWLEDGMENT

M.A. is a Georg Forster fellow of the Alexander von Humboldt Foundation and gratefully acknowledges this support. The authors would like to thank Dr. Karl Fischer for very helpful discussions.

REFERENCES AND NOTES

1 J. P. Gong, Y. Katsuyama, T. Kurokawa, Y. Osada, *Adv. Mater.* **2003**, *15*, 1155.

2 J. P. Gong, *Soft Matter* **2010**, *6*, 2583.

3 J. A. Neal, D. Mozhdehi, Z. Guan, *J. Am. Chem. Soc.* **2015**, *137*, 4846.

4 J.-Y. Sun, X. Zhao, W. R. Illeperuma, O. Chaudhuri, K. H. Oh, D. J. Mooney, J. J. Vlassak, Z. Suo, *Nature* **2012**, *489*, 133.

5 L. Brunsveld, B. J. Folmer, E. W. Meijer, R. Sijbesma, *Chem. Rev.* **2001**, *101*, 4071.

6 S. Seiffert, *Prog. Polym. Sci.* **2017**, *66*, 1.

7 K. Dušek, W. Prins, "Structure and elasticity of non-crystalline polymer networks." Fortschritte der Hochpolymeren-Forschung. Springer, Berlin, Heidelberg, **1969**, 1-102.

8 S. Panyukov, Y. Rabin, *Phys. Rep.* **1996**, *269*, 1.

9 M. Shibayama, *Macromol. Chem. Phys.* **1998**, *199*, 1.

10 T. Sakai, T. Matsunaga, Y. Yamamoto, C. Ito, R. Yoshida, S. Suzuki, N. Sasaki, M. Shibayama, U.-i. Chung, *Macromolecules* **2008**, *41*, 5379.

11 T. Sakai, Y. Akagi, S. Kondo, U. Chung, *Soft Matter* **2014**, *10*, 6658.

12 Y. Akagi, J. P. Gong, U.-i. Chung, T. Sakai, *Macromolecules* **2013**, *46*, 1035.

13 Y. Akagi, T. Katashima, Y. Katsumoto, K. Fujii, T. Matsunaga, U.-i. Chung, M. Shibayama, T. Sakai, *Macromolecules* **2011**, *44*, 5817.

14 T. Rossow, A. Habicht, S. Seiffert, *Macromolecules* **2014**, *47*, 6473.

15 T. Rossow, S. Seiffert, *Polym. Chem.* **2014**, *5*, 3018.

16 S. Tang, A. Habicht, S. Li, S. Seiffert, B. D. Olsen, *Macromolecules* **2016**, *49*, 5599.

17 W. C. Yount, D. M. Loveless, S. L. Craig, *J. Am. Chem. Soc.* **2005**, *127*, 14488.

18 W. C. Yount, D. M. Loveless, S. L. Craig, *Angew. Chem. Int. Ed.* **2005**, *44*, 2746.

19 E. A. Appel, F. Biedermann, D. Hoogland, J. Del Barrio, M. D. Driscoll, S. Hay, D. J. Wales, O. A. Scherman, *J. Am. Chem. Soc.* **2017**, *139*, 12985.

20 E. A. Appel, R. A. Forster, A. Koutsioubas, C. Toprakcioglu, O. A. Scherman, *Angew. Chem.* **2014**, *126*, 10202.

21 C. S. Y. Tan, G. Agmon, J. Liu, D. Hoogland, E.-R. Janeček, E. A. Appel, O. A. Scherman, *Polym. Chem.* **2017**, *8*, 5336.

22 S. Tang, B. D. Olsen, *Macromolecules* **2016**, *49*, 9163.

23 T. Hiroi, S. Kondo, T. Sakai, E. P. Gilbert, Y.-S. Han, T.-H. Kim, M. Shibayama, *Macromolecules* **2016**, *49*, 4940.

24 H. Kamata, Y. Akagi, Y. Kayasuga-Kariya, U.-i. Chung, T. Sakai, *Science* **2014**, *343*, 873.

25 S. Kondo, T. Hiroi, Y. S. Han, T. H. Kim, M. Shibayama, U. i. Chung, T. Sakai, *Adv. Mater.* **2015**, *27*, 7407.

26 P. Lin, S. Ma, X. Wang, F. Zhou, *Adv. Mater.* **2015**, *27*, 2054.

27 M. Zhong, Y.-T. Liu, X.-Y. Liu, F.-K. Shi, L.-Q. Zhang, M.-F. Zhu, X.-M. Xie, *Soft Matter* **2016**, *12*, 5420.

28 J. Liu, C. S. Y. Tan, Z. Yu, Y. Lan, C. Abell, O. A. Scherman, *Adv. Mater.* **2017**, *29*, 1604951.

29 M. Guo, L. M. Pitet, H. M. Wyss, M. Vos, P. Y. Dankers, E. Meijer, *J. Am. Chem. Soc.* **2014**, *136*, 6969.

30 X. Hu, M. Vatankhah-Varnoosfaderani, J. Zhou, Q. Li, S. S. Sheiko, *Adv. Mater.* **2015**, *27*, 6899.

31 M. Ahmadi, L. Löser, K. Fischer, K. Saalwächter, S. Seiffert, *Macromol. Chem. Phys.*, *2020*, 1900400. https://doi.org/10.1002/macp.201900400.

32 S. Czarnecki, T. Rossow, S. Seiffert, *Polymers* **2016**, *8*, 82.

33 D. L. Elbert, J. A. Hubbell, *Biomacromolecules* **2001**, *2*, 430.

34 R. Shunmugam, G. J. Gabriel, K. A. Aamer, G. N. Tew, *Macromol. Rapid Commun.* **2010**, *31*, 784.

35 A. Habicht, S. Czarnecki, T. Rossow, S. Seiffert, *J. Polym. Sci. B* **2017**, *55*, 19.

36 G. Hauser, S. Seiffert, W. Oppermann, *J. Microsc.* **2008**, *230*, 353.

37 T. Miron, M. Wilchek, *Bioconjug. Chem.* **1993**, *4*, 568.

38 H. Goldansaz, Q. Voleppe, S. Pioge, C.-A. Fustin, J.-F. Gohy, J. Brassinne, D. Auhl, E. Van Ruymbeke, *Soft Matter* **2015**, *11*, 762.

39 R. Wang, M. Geven, P. J. Dijkstra, P. Martens, M. Karperien, *Soft Matter* **2014**, *10*, 7328.

40 I. M. Henderson, R. C. Hayward, *Polym. Chem.* **2012**, *3*, 1221.

41 R. Holyer, C. Hubbard, S. Kettle, R. Wilkins, *Inorg. Chem.* **1966**, *5*, 622.

42 K. Nishi, K. Fujii, Y. Katsumoto, T. Sakai, M. Shibayama, *Macromolecules* **2014**, *47*, 3274.

43 M. Ahmadi, L. G. Hawke, H. Goldansaz, E. Van Ruymbeke, *Macromolecules* **2015**, *48*, 7300.

44 M. Ahmadi, A. Jangizehi, E. Van Ruymbeke, S. Seiffert, *Macromolecules* **2019**, *52*, 5255.

45 Q. Chen, G. J. Tudryn, R. H. Colby, *J. Rheol.* **2013**, *57*, 1441.

46 A. E. Likhtman, T. C. McLeish, *Macromolecules* **2002**, *35*, 6332.

47 M. Ahmadi, C. Bailly, R. Keunings, M. Nekoomanesh, H. Arabi, E. Van Ruymbeke, *Macromolecules* **2011**, *44*, 647.

48 M. Ahmadi, S. Pioge, C.-A. Fustin, J.-F. Gohy, E. Van Ruymbeke, *Soft Matter* **2017**, *13*, 1063.

49 J. E. Jam, M. Nekoomanesh, M. Ahmadi, H. Arabi, *Iran. Polym. J.* **2012**, *21*, 403.

50 W. Schmolke, M. Ahmadi, S. Seiffert, *Phys. Chem. Chem. Phys.* **2019**, *21*, 19623.

51 G. Cui, V. A. Boudara, Q. Huang, G. P. Baeza, A. J. Wilson, O. Hassager, D. J. Read, J. Mattsson, *J. Rheol.* **2018**, *62*, 1155.

52 F. Lange, K. Schwenke, M. Kurakazu, Y. Akagi, U.-i. Chung, M. Lang, J.-U. Sommer, T. Sakai, K. Saalwächter, *Macromolecules* **2011**, *44*, 9666.

53 P. Thordarson, *Chem. Soc. Rev.* **2011**, *40*, 1305.

54 A. Jangizehi, M. Ahmadi, S. Seiffert, *J. Polym. Sci. B* **2019**, *57*, 1209.

55 A. Jangizehi, S. R. Ghaffarian, M. Ahmadi, *Polym. Adv. Technol.* **2018**, *29*, 726.

56 F. J. Stadler, W. Pyckhout-Hintzen, J.-M. Schumers, C.-A. Fustin, J.-F. Gohy, C. Bailly, *Macromolecules* **2009**, *42*, 6181.

57 H. Goldansaz, A. Jangizehi, G. Nikravan, O. Verkinderen, B. Goderis, S. R. Ghaffarian, E. van Ruymbeke, M. Ahmadi, *React. Funct. Polym.* **2019**, *137*, 27.

58 Y. L. Rao, V. Feig, X. Gu, G. J. Nathan Wang, Z. Bao, *J. Polym. Sci. A Polym. Chem.* **2017**, *55*, 3110.

59 S. Seiffert, W. Oppermann, *J. Microsc.* **2005**, *220*, 20.